

# The Combination of S[?]N and S[?]Cl Noncovalently Conformational Locks for Constructing High-Planarity and Low-Cost Non-fused-Ring Electron Acceptors

Ziyang Han<sup>1</sup>, Congqi Li<sup>1</sup>, Xiaobin Gu<sup>1</sup>, Xiao Han<sup>1</sup>, Sixuan Wang<sup>1</sup>, Yanan Wei<sup>1</sup>, Jinhua Gao<sup>1</sup>, Zhixiang Wei<sup>2</sup>, Yunhao Cai<sup>1</sup>, Xin Zhang<sup>1</sup>, and Hui Huang<sup>1</sup>

<sup>1</sup>University of the Chinese Academy of Sciences

<sup>2</sup>National Center for Nanoscience and Technology

February 6, 2023

## Abstract

By employing thiazole and 4-chlorothiazole as the A' units, two A-D-A'-D-A type nonfused-ring electron acceptors (NFREAs) **Tz-H** and **Tz-Cl** were designed and synthesized. Replacing thiazole in **Tz-H** with 4-chlorothiazole can not only remarkably shorten the synthetic route through C-H direct arylation but also enhance molecular planarity with the simultaneous incorporation of S...N and S...Cl non-covalently conformational locks (NoCLs). The photovoltaic devices based on PM6:**Tz-Cl** exhibited a power conversion efficiency as high as 11.10%, much higher than that of PM6:**Tz-H** (6.41%), mainly due to more efficient exciton dissociation, better and more balanced carrier mobility, less charge recombination, and more favorable morphology. These findings demonstrate the great potential of NoCLs in achieving low-cost and high-performance NFREAs.

**Cite this paper:** *Chin. J. Chem.* **2022**, *40*, XXX—XXX. DOI: [10.1002/cjoc.202200XXX](https://doi.org/10.1002/cjoc.202200XXX)

The Combination of S[?]N and S[?]Cl Noncovalently Conformational Locks for Constructing High-Planarity and Low-Cost Nonfused-Ring Electron Acceptors<sup>†</sup>

Ziyang Han,<sup>a</sup> Congqi Li,<sup>a</sup> Xiaobin Gu,<sup>a</sup> Xiao Han,<sup>a</sup> Sixuan Wang,<sup>a</sup> Yanan Wei,<sup>a</sup> Jinhua Gao,<sup>a</sup> Zhixiang Wei,<sup>b</sup> Yunhao Cai,<sup>a</sup> Xin Zhang\*,<sup>a</sup> and Hui Huang\*,<sup>a</sup>

<sup>a</sup> College of Materials Science and Opto-Electronic Technology & Center of Materials Science and Opto-electronics Engineering & CAS Center for Excellence in Topological Quantum Computation & CAS Key Laboratory of Vacuum Physics, University of Chinese Academy of Sciences, Beijing 100049, China<sup>b</sup> Center for Excellence in Nanoscience (CAS) & Key Laboratory of Nanosystem and Hierarchical Fabrication (CAS), National Center for Nanoscience and Technology, Beijing 100190, China

---

## Comprehensive Summary

By employing thiazole and 4-chlorothiazole as the A' units, two A-D-A'-D-A type nonfused-ring electron acceptors (NFREA

---

## Keywords

Organic solar cells | Nonfused-ring electron acceptors | Noncovalently conformational locks | High-planarity and low-cost ac

---

## Background and Originality Content

In recent years, the development of organic solar cells (OSCs) has largely benefited from the revolution of non-fullerene acceptors, especially fused-ring electron acceptors (FREAs) with the acceptor-donor-acceptor (A-D-A) architecture, which were pioneered by Zhan et al. in 2015.<sup>[1-3]</sup> Later in early 2019, Zou et al. reported a new generation of A-DA'D-A structured FREAs (represented by Y6), containing electron-deficient units in the fused-ring cores.<sup>[4, 5]</sup> Due to the unique structural feature, FREAs possess superior absorption property and tight intermolecular  $\pi$ - $\pi$  stacking in common.<sup>[6]</sup> With the continuous efforts on molecular tailoring and device engineering, the power conversion efficiencies (PCEs) of the state-of-the-art single junction OSCs have exceeded 19%.<sup>[7-14]</sup> However, due to the remarkable structural feature of highly fused conjugated backbones, FREAs generally require complicated synthetic approaches and suffer from low yields and high product costs, which may severely hinder their large-scale applications.

To address the disadvantage of FREAs, an alternative strategy for low-cost electron acceptors was proposed, namely nonfused-ring electron acceptors (NFREAs).<sup>[15]</sup> In general, this novel type of acceptors shares an unfused central core (a simply fused or even completely unfused  $\pi$ -conjugated core), thus making the synthesis route more concise.<sup>[16-21]</sup> More importantly, the noncovalently conformational locks (NoCLs) strategy is generally introduced in the molecular design of NFREAs, which can effectively restrict the rotation of single bonds and reduce conformational isomers raised from the unfused-ring cores, thus improving the molecular planarity and rigidity.<sup>[22-26]</sup> Therefore, NFREAs possess a simple-structured yet co-planar conjugated backbone, opening the opportunity for constructing cost-effective acceptor materials.<sup>[27-29]</sup> Regarded as tailoring from A-DA'D-A type FREAs, A-D-A'-D-A structured NFREAs have received much attention recently. Due to the key role of the A' unit in regulating light-harvest ability, energy levels, intramolecular conformation, and intermolecular packing behaviors, a lot of work has been devoted to the selection of A' units, including benzo[*c*][1,2,5]thiadiazole,<sup>[30, 31]</sup> 2*H*-benzo[*d*][1,2,3]triazole,<sup>[32, 33]</sup> thieno[3,4-*c*]pyrrole-4,6-dione,<sup>[34, 35]</sup> and benzo-[1,2-*c*:4,5-*c'*]dithiophene-4,8-dione.<sup>[36, 37]</sup> However, it is still challenging to rationally choose an electron-withdrawing motif as the A' unit.

Thiazole is a widely-used electron-deficient heteroaromatic ring due to its electron-withdrawing nitrogen of imine (C=N),<sup>[38]</sup> which has been employed in constructing organic semiconductors for optoelectronics, such as OSCs,<sup>[39]</sup> organic field-effect transistors (OFETs),<sup>[40]</sup> and organic light-emitting diodes (OLEDs).<sup>[41]</sup> Compared with thiazole, 4-chlorothiazole should be a more electron-deficient unit, which is expected to build organic conjugated molecules with deep-lying highest occupied molecular orbital (HOMO) energy levels. Particularly, the N and Cl atoms in 4-chlorothiazole may be able to form S...N and S...Cl NoCLs with neighboring thiophene units to enhance the molecular planarity. Therefore, 4-chlorothiazole is an excellent candidate as the A' unit to construct high-planarity and low-cost NFREAs.

Herein, thiazole and 4-chlorothiazole were utilized as the A' units to construct two A-D-A'-D-A type NFREAs, namely **Tz-H** and **Tz-Cl**, respectively (Figure 1a). Compared with **Tz-H**, **Tz-Cl** possessed a facile and concise synthesis, due to the unexpectedly C-H direct arylation of 2,5-dibromo-4-chlorothiazole. Both density function theory (DFT) calculations and single-crystal X-ray diffraction (SC-XRD) data revealed that the simultaneous incorporation of S...N and S...Cl NoCLs can provide a more planar conjugated backbones, and thus a more compact and ordered packing than the sole introduction of S...N NoCLs. When blending with the polymer donor PM6, the **Tz-Cl**-based blend film afforded higher exciton dissociation efficiency, more balanced charge mobility, lower recombination loss, shorter charge extraction time, and more favorable morphology. Therefore, a PCE of 11.10% was achieved for **Tz-Cl**-based devices, much higher than that of the **Tz-H** counterpart (6.41%). This work demonstrated the potential of NoCLs to construct low-cost NFREAs.

## Results and Discussion

### Synthesis and characterization

The synthesis routes of the two NFREAs were shown in Scheme S1, and the detailed synthesis procedures,  $^1\text{H}$ -/ $^{13}\text{C}$ -NMR spectrometry, and mass spectrometry were given in Supporting Information. Initially, we tried to obtain the dialdehyde intermediate **4** from 2,5-dibromothiazole (**1**) and compound **6** by Pd(0)-catalyzed C-H activation, but failed. Thus, we utilized compound **1** with 2 equivalents of mono-organotin compound (**2**) to afford a nonfused-type conjugated core (**3**), followed by the Vilsmeier-Haack reaction to convert dialdehyde intermediate **4**. Different from the chloro-free thiazole derivation, 2,5-dibromo-4-chlorothiazole (**5**) can unexpectedly undergo a two-fold C-H activation with compound **6** to directly afford dialdehyde intermediate **7**. Finally, **Tz-H** and **Tz-Cl** was obtained through Knoevenagel condensation between the dialdehyde intermediate (**4** or **7**) and 2-(5,6-dichloro-3-oxo-2,3-dihydro-1*H*-inden-1-ylidene)malononitrile (IC-2Cl). Obviously, the synthetic route for **Tz-Cl** is more concise, which may be beneficial to reducing the production cost. Both **Tz-H** and **Tz-Cl** showed good solubility in common organic solvents, such as chloroform, tetrahydrofuran, and chlorobenzene.

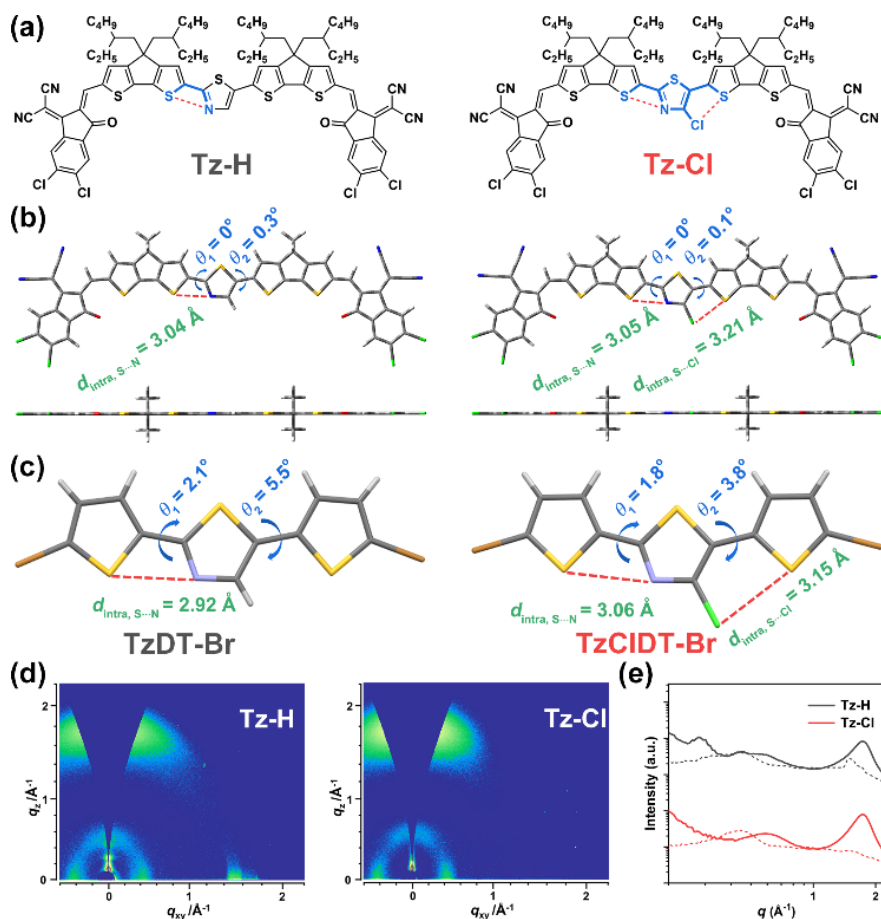


**Figure 1** (a) Chemical structures and (b) optimized geometries (top: top view; bottom: side view) of the two NFREAs. (c) Single crystal structures of the two model compounds **TzDT-Br** and **TzCIDT-Br**. (d) GIWAXS patterns of neat **Tz-H** and **Tz-Cl** films and (e) the corresponding scattering profiles in the out-of-plane (solid line) and in-plane (dashed line) directions.

The optimized molecular geometries of **Tz-H** and **Tz-Cl** with simplified side-chains were investigated with DFT calculations at the B3LYP/6-31G(d,p) level. As shown in Figure 1b, both **Tz-H** and **Tz-Cl** possessed near-coplanar  $\pi$ -conjugated backbones with small dihedral angles ( $\theta_1$  and  $\theta_2$ ). Especially, **Tz-Cl** exhibited

both  $\theta_1$  and  $\theta_2$  of near  $0^\circ$ , which is favorable for the intermolecular  $\pi$ - $\pi$  stacking and charge transport. The intramolecular distance between the sulfur and nitrogen atoms ( $d_{\text{intra, S}\cdots\text{N}}$ ) were calculated to be  $\sim 3.04$  and  $\sim 3.05$  Å for **Tz-H** and **Tz-Cl**, respectively, and the intramolecular distance between the sulfur and chlorine atoms ( $d_{\text{intra, S}\cdots\text{Cl}}$ ) was calculated to be  $\sim 3.21$  Å for **Tz-Cl**, much shorter than the sum of the van der Waals radius ( $r_{\text{w, S}\cdots\text{N}} = 3.35$  Å and  $r_{\text{w, S}\cdots\text{Cl}} = 3.65$  Å), indicating the existence of S $\cdots$ N and S $\cdots$ Cl NoCLs. Thus, **Tz-Cl** possessed a more planar conformation mainly due to the incorporation of multiple NoCLs.

To gain more structural information on the thiazole- and 4-chlorothiazole-based NFREAs, the single crystals of two model compounds TzDT-Br and TzClDT-Br were grown by solvent vapor diffusion using chloroform/methanol (Table S1). As shown in Figure 1c, the single crystal structure of TzClDT-Br shared a more co-planar conformation with dihedral angles  $\theta_1$  of  $1.8^\circ$  and  $\theta_2$  of  $3.8^\circ$ , much smaller than those of  $2.1^\circ$  and  $5.5^\circ$  in TzDT-Br. In addition, the short  $d_{\text{intra, S}\cdots\text{N}}$  and  $d_{\text{intra, S}\cdots\text{Cl}}$  again indicated that the planar conformations could be enforced by S $\cdots$ N and S $\cdots$ Cl NoCLs. Such a planar conjugated backbone of TzClDT-Br is expected to favor the stacking of **Tz-Cl**.

**Table 1** Basic properties of **Tz-H** and **Tz-Cl**

| NFREAs       | $\lambda_{\text{abs.max}}^{\text{sol.}}$ [nm] | $\lambda_{\text{abs.max}}^{\text{film}}$ [nm] | $E_g^{\text{opt}}$ [eV] | $E_{\text{HOMO}}/E_{\text{LUMO}}$ [eV] |
|--------------|---|---|-------------------------|--|
| <b>Tz-H</b>  | 717   | 711, 780                                      | 1.41                    | -5.61/-3.94                            |
| <b>Tz-Cl</b> | 718   | 700, 768                                      | 1.43                    | -5.65/-3.97                            |

The packing behavior in the neat films were investigated by two-dimensional grazing incidence wide-angle X-ray scattering (2D-GIWAXS). As shown in Figures 1c and 1d, the neat film of **Tz-H** exhibited a bi-modal packing as supported by the (010)  $\pi$ - $\pi$  stacking peaks ( $d_{010} = 3.61$  Å) along both the out-of-plane (OOP) and the in-plane (IP) directions. In contrast, a dominant (010)  $\pi$ - $\pi$  stacking peak in the OOP direction ( $q_z = 1.75$  Å $^{-1}$ ,  $d_{010} = 3.58$  Å) was observed in the **Tz-Cl** thin film, indicating a predominantly face-on orientation. Besides, the crystal coherence lengths (CCLs) for (010) diffraction peaks along the OOP direction were 1.65 and 1.82 nm for **Tz-H** and **Tz-Cl**, respectively, as determined by the Scherrer equation. The reduced  $\pi$ - $\pi$  stacking distance and enhanced CCLs in the neat film of **Tz-Cl** indicated a more compact and ordered packing, which may be attributed to the improved backbone coplanarity by the simultaneous incorporation of S $\cdots$ N and S $\cdots$ Cl NoCLs.

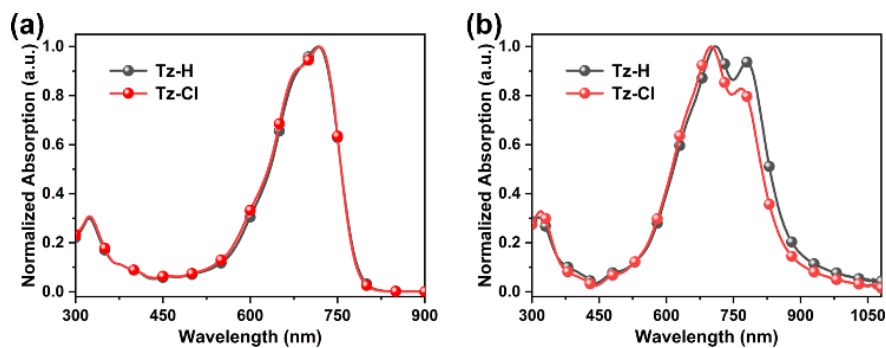


**Figure 2** Normalized dilute solution (a) and thin film (b) optical absorption spectra of **Tz-H** and **Tz-Cl**.

The UV-vis absorption spectra of the two NFREAs in dilute chloroform solution and thin film were shown in Figures 2a and 2b, and the corresponding optical parameters were summarized in Table 1. Due to their similar chemical structures, both **Tz-H** and **Tz-Cl** exhibited almost identical solution absorption spectra with the maximum peaks located at 717 and 718 nm, respectively. In solid state, **Tz-H** and **Tz-Cl** possessed a strong absorption in the region of 600-850 nm, showing a red-shift of  $\sim 50$  nm relative to that in solution

state (724 nm). Specially in the  $S_0$ - $S_1$  band, the absorption intensity of 0–0 vibronic transition was relatively lower than that of 0–1 transition, indicating the formation of H-aggregates in the two NFREA films.<sup>[42]</sup> The optical bandgaps of **Tz-H** and **Tz-Cl** were 1.41 and 1.43 eV, respectively, according to the equation:  $E_g^{\text{opt}} = 1240/\lambda_{\text{onset}}$ . According to the cyclic voltammetry (CV) measurements, the HOMO and the lowest unoccupied molecular orbital (LUMO) energy levels of **Tz-H** and **Tz-Cl** were estimated to be -5.62/-3.94 and -5.65/-3.97 eV, respectively (Figure S1 and Table 1). Compared with **Tz-H**, **Tz-Cl** possessed slightly lower-lying HOMO/LUMO energy levels, which should be attributed to the introduction of electron-withdrawing chlorine atom.

### Photovoltaic properties

To investigate the photovoltaic performance of the two NFREAs, OSC devices with a conventional device structure of ITO/PEDOT:PSS/active layer/PDIN/Ag based on PM6:**Tz-H** and PM6:**Tz-Cl** blends were fabricated. The detailed optimization process of **Tz-H** - and **Tz-Cl** -based photovoltaic devices was shown in Tables S2 and S3, including the weight ratio of donor and acceptor as well as the content of additive. The optimized device based on PM6:**Tz-H** showed an inferior PCE of 6.41%, with an open-circuit voltage ( $V_{\text{oc}}$ ) of 0.838 V, a short-circuit current density ( $J_{\text{sc}}$ ) of 15.74 mA cm<sup>-2</sup>, and a fill factor (FF) of 48.57% (Figure 3a and Table 2). Impressively, **Tz-Cl** -based device exhibited a much higher PCE of 11.10%, with simultaneously improved  $V_{\text{oc}}$  (0.841 V),  $J_{\text{sc}}$  (20.71 mA cm<sup>-2</sup>), and FF (63.72%). To further confirm the accuracy of the  $J_{\text{sc}}$  values, the external quantum efficiency (EQE) spectra of the devices were shown in Figure 3b. The integrated  $J_{\text{sc}}$  values obtained from the EQE responses were 15.61 and 20.27 mA cm<sup>-2</sup> for **Tz-H** - and **Tz-Cl** -based devices, respectively, which were well consistent with the  $J$  -  $V$  measurements.

**Table 2** Photovoltaic parameters of OSCs based on PM6:NFREAs under AM1.5G illumination, 100 mW cm<sup>-2</sup>.

| Active layers     | $V_{\text{oc}}^a$ [V] | $J_{\text{sc}}$ [mA cm <sup>-2</sup> ] | FF [%]             | PCE [%]            |
|-------------------|-----------------------|--|--------------------|--------------------|
| PM6: <b>Tz-H</b>  | 0.838 (0.840±0.001)   | 15.74 (15.79±0.29)                     | 48.57 (46.80±1.23) | 6.41 (6.20±0.11)   |
| PM6: <b>Tz-Cl</b> | 0.841 (0.840±0.001)   | 20.71 (20.73±0.44)                     | 63.72 (62.66±1.23) | 11.10 (10.91±0.12) |

<sup>a</sup> The average values shown in parentheses were obtained from 15 devices.

To further understand the changes in above-mentioned photovoltaic properties, charge dynamics were systematically investigated. The photocurrent density ( $J_{\text{ph}}$ ) versus effective voltage ( $V_{\text{eff}}$ ) curves were firstly measured to explore the charge generation and extraction mechanism. Generally,  $J_{\text{ph}}$  is defined as  $J_{\text{L}} - J_{\text{D}}$ , where  $J_{\text{L}}$  and  $J_{\text{D}}$  are the photocurrent densities under illumination and in the dark conditions, respectively.  $V_{\text{eff}}$  can be defined as  $V_{\text{eff}} = V_0 - V_{\text{bias}}$ , where  $V_0$  is the voltage at which  $J_{\text{ph}} = 0$  and  $V_{\text{bias}}$  is the applied voltage.<sup>[43]</sup> Thus, the exciton dissociation probability can be calculated as the ratio of  $J_{\text{ph}}/J_{\text{sat}}$ , where  $J_{\text{sat}}$  is the saturation photocurrent density. As shown in Figure 3c, the  $P_{\text{diss}}$  values of **Tz-H** - and **Tz-Cl** -based devices were calculated to be 91.7% and 96.1%, respectively. The results demonstrated that the **Tz-Cl** -based device exhibited a higher exciton dissociation efficiency, which was well consistent with the higher  $J_{\text{sc}}$  value of 20.71 mA cm<sup>-2</sup>.

To investigate the charge transport properties in the active layers, hole and electron mobilities were measured by the space charge limited current (SCLC) method. As shown in Figure S2, the hole ( $\mu_{\text{h}}$ ) and electron ( $\mu_{\text{e}}$ ) mobilities of **Tz-H** -based blend film were estimated to be  $2.35 \times 10^{-5}$  and  $4.06 \times 10^{-5}$  cm<sup>2</sup> V<sup>-1</sup> s<sup>-1</sup> with a  $\mu_{\text{h}}/\mu_{\text{e}}$  ratio of 0.58. In contrast, **Tz-Cl** -based blend film exhibited not only enhanced ( $5.54 \times 10^{-5}$  and  $5.47 \times 10^{-5}$  cm<sup>2</sup> V<sup>-1</sup> s<sup>-1</sup>) but also balanced ( $\mu_{\text{h}}/\mu_{\text{e}} = 1.01$ ) charge mobilities, which contributed to the observed higher  $J_{\text{sc}}$  and FF in the PM6:**Tz-Cl** -based photovoltaic device. In addition, the charge recombination process was investigated by measuring the light intensity ( $P_{\text{light}}$ ) dependent  $J_{\text{sc}}$ . The relationship between  $P_{\text{light}}$  and  $J_{\text{sc}}$  follows the formula of  $J_{\text{sc}} \propto P_{\text{light}}^a$ . The exponent  $a$  value approaches to unit, when free charge carriers are almost swept out and collected at the electrodes. As shown in Figure 3d, the  $a$  value was estimated to be 0.952 for the **Tz-Cl** -based device under the short-circuit condition, which is a little higher

than that of PM6:Tz-H (0.927). The higher  $\alpha$  for the Tz-Cl-based device indicated its weaker bimolecular recombination that may contribute to the higher  $J_{sc}$  and FF relative to the Tz-H-based device.

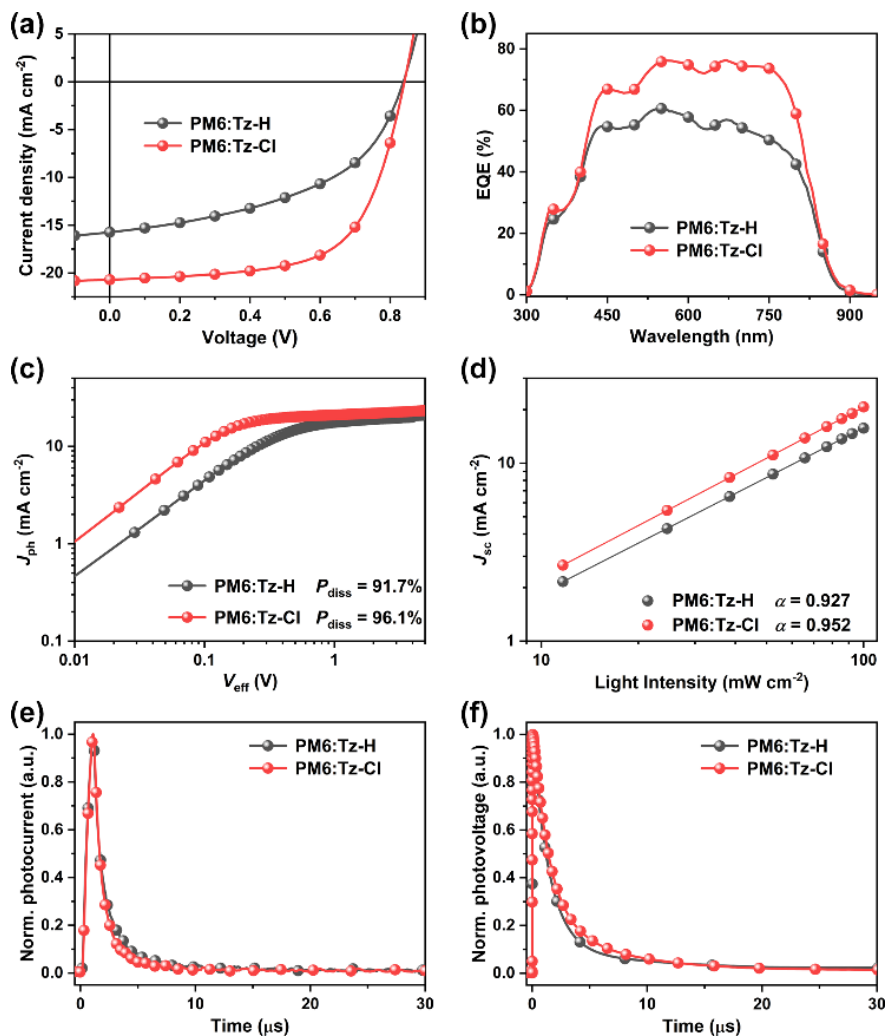


**Figure 3** (a)  $J-V$  characteristics, (b) EQE responses, (c)  $J_{ph}-V_{eff}$ , (d)  $J_{sc}-P_{light}$ , (e) TPC, and (f) TPV measurements of the optimized OSCs based on PM6:Tz-H and PM6:Tz-Cl .

To further understand the charge recombination and extraction processes, transient photocurrent (TPC) and transient photovoltage (TPV) measurements were carried out. As presented in Figure 3e, the charge sweep-out times under the short-circuit condition were roughly estimated to be 0.97 and 0.84  $\mu\text{s}$ , while the charge carrier lifetimes obtained from the decay traces of TPV measurements (Figure 3f) were 1.59 and 1.83  $\mu\text{s}$  for Tz-H - and Tz-Cl -based devices, respectively. The shorter charge extraction time can be attributed to the higher electron mobility, and the relatively longer lifetime of free carriers at open-circuit voltage may indicate less recombination in the Tz-Cl -based device.

#### Film morphology

To evaluate the miscibility between the two NFREAs and PM6, Flory-Huggins interaction parameters ( $\chi$ ) were estimated by using contact angle measurements. The contact angles of two liquids (deionized water and ethylene glycol) on the neat PM6, Tz-H , and Tz-Cl films were investigated (Figure 4a). The surface

tensions ( $\gamma$ ) of PM6, **Tz-H**, and **Tz-Cl** were calculated to be 19.75, 26.02, and 23.90 mN m<sup>-1</sup>, respectively (Table S4). According to the empirical equation  $\chi = K(\sqrt{\gamma_D} - \sqrt{\gamma_A})^2$ , where  $K$  is a constant, the  $\chi_{\text{PM6:Tz-H}}$  and  $\chi_{\text{PM6:Tz-Cl}}$  were 0.43 and 0.19 $K$ , respectively, indicating a better D/A miscibility for the PM6:**Tz-Cl** blend film.

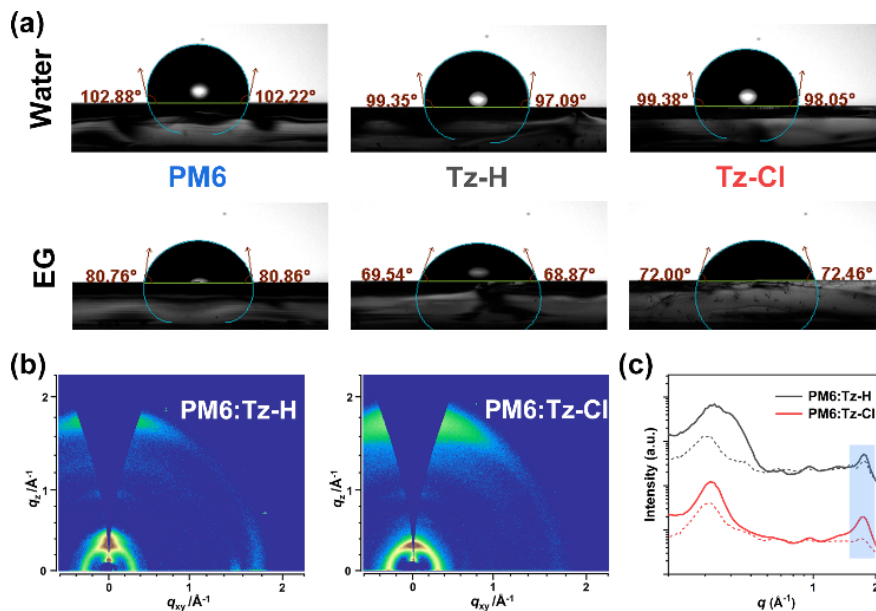


**Figure 4** (a) Water and ethylene glycol (EG) contact angles of the neat PM6, **Tz-H**, and **Tz-Cl** surfaces. (b) GIWAXS patterns of PM6:**Tz-H** and PM6:**Tz-Cl** blend films and (c) the corresponding scattering profiles in the out-of-plane (solid line) and in-plane (dashed line) directions.

The bulk morphologies of blend films were investigated by transmission electron microscopy (TEM). It is obvious that the PM6:**Tz-Cl** blend possessed a smaller domain size and nano-scale phase separation (Figure S3), which is well consistent with the results of surface energy. GIWAXS measurements were further utilized to investigate the morphological feature of the two blend films. As shown in Figure 4b, face-on and edge-on crystallites coexisted in the PM6:**Tz-H** blend film, which is similar to the neat **Tz-H** film. Compared with the bimodal texture of the PM6:**Tz-H** blend film, the PM6:**Tz-Cl** blend film exhibited predominant face-on orientation, which is beneficial to the charge transport in vertical direction (Figure 4c). As discussed above, these morphological features indicated that the **Tz-Cl**-based blend film exhibited a more favorable morphology, which might be a crucial reason for achieving better photovoltaic performance.

## Conclusions

In conclusion, the electron-deficient units, thiazole and 4-chlorothiazole, were employed to construct two NFREAs, **Tz-H** and **Tz-Cl**, respectively. Compared with **Tz-H**, **Tz-Cl** possessed a highly-planar backbone, ascribed to the simultaneous incorporation of S...N and S...Cl NoCLs. The **Tz-Cl**-based device delivered a PCE of 11.10%, much higher than the **Tz-H**-based control device (6.41%), mainly due to more efficient exciton dissociation, better and more balanced carrier mobility, less charge recombination, and more favorable morphology. Thus, this work provides an effective strategy for designing high-planarity and low-cost NFREAs via the incorporation of multiple NoCLs.

## Supporting Information

The supporting information for this article is available on the WWW under <https://doi.org/10.1002/cjoc.2021xxxxx>.

## Acknowledgement

Z. Han and C. Li contributed equally to this work. The authors acknowledge the financial support from the National Natural Science Foundation of China (51925306, 52103352, and 52120105006), National Key R&D Program of China (2018FYA 0305800), Key Research Program of Chinese Academy of Sciences (XDPB08-2), the Strategic Priority Research Program of Chinese Academy of Sciences (XDB28000000), the Youth Innovation Promotion Association of Chinese Academy of Sciences (2022165), and the Fundamental Research Funds for the Central Universities. DFT results described in this report were obtained from the National Supercomputing Center in Shenzhen (Shenzhen Cloud Computing Center).

## References

- [1] Wang, J., Zhan, X. From Perylene Diimide Polymers to Fused-Ring Electron Acceptors: A 15-Year Exploration Journey of Nonfullerene Acceptors. *Chin. J. Chem.* **2022**, *40*, 1592-1607. [2] Zhang, G.; Zhao, J.; Chow, P. C. Y.; Jiang, K.; Zhang, J.; Zhu, Z.; Zhang, J.; Huang, F., Yan, H. Nonfullerene Acceptor Molecules for Bulk Heterojunction Organic Solar Cells. *Chem. Rev.* **2018**, *118*, 3447-3507. [3] Lin, Y.; Wang, J.; Zhang, Z.-G.; Bai, H.; Li, Y.; Zhu, D., Zhan, X. An Electron Acceptor Challenging Fullerenes for Efficient Polymer Solar Cells. *Adv. Mater.* **2015**, *27*, 1170-1174. [4] Wei, Q.; Liu, W.; Leclerc, M.; Yuan, J.; Chen, H., Zou, Y. A-DA'D-A non-fullerene acceptors for high-performance organic solar cells. *Sci. China Chem.* **2020**, *63*, 1352-1366. [5] Yuan, J.; Zhang, Y.; Zhou, L.; Zhang, G.; Yip, H.-L.; Lau, T.-K.; Lu, X.; Zhu, C.; Peng, H.; Johnson, P. A.; Leclerc, M.; Cao, Y.; Ulanski, J.; Li, Y., Zou, Y. Single-Junction Organic Solar Cell with over 15% Efficiency Using Fused-Ring Acceptor with Electron-Deficient Core. *Joule* **2019**, *3*, 1140-1151. [6] Hou, J.; Inganäs, O.; Friend, R. H., Gao, F. Organic solar cells based on non-fullerene acceptors. *Nat. Mater.* **2018**, *17*, 119-128. [7] Zhu, L.; Zhang, M.; Xu, J.; Li, C.; Yan, J.; Zhou, G.; Zhong, W.; Hao, T.; Song, J.; Xue, X.; Zhou, Z.; Zeng, R.; Zhu, H.; Chen, C.-C.; MacKenzie, R. C. I.; Zou, Y.; Nelson, J.; Zhang, Y.; Sun, Y., Liu, F. Single-junction organic solar cells with over 19% efficiency enabled by a refined double-fibril network morphology. *Nat. Mater.* **2022**, *21*, 656-663. [8] Sun, R.; Wu, Y.; Yang, X.; Gao, Y.; Chen, Z.; Li, K.; Qiao, J.; Wang, T.; Guo, J.; Liu, C.; Hao, X.; Zhu, H., Min, J. Single-Junction Organic Solar Cells with 19.17% Efficiency Enabled by Introducing One Asymmetric Guest Acceptor. *Adv. Mater.* **2022**, *34*, 2110147. [9] Cui, Y.; Xu, Y.; Yao, H.; Bi, P.; Hong, L.; Zhang, J.; Zu, Y.; Zhang, T.; Qin, J.; Ren, J.; Chen, Z.; He, C.; Hao, X.; Wei, Z., Hou, J. Single-Junction Organic Photovoltaic Cell with 19% Efficiency. *Adv. Mater.* **2021**, *33*, 2102420. [10] Wei, Y.; Chen, Z.; Lu, G.; Yu, N.; Li, C.; Gao, J.; Gu, X.; Hao, X.; Lu, G.; Tang, Z.; Zhang, J.; Wei, Z.; Zhang, X., Huang, H. Binary Organic Solar Cells Breaking 19% via Manipulating the Vertical Component Distribution. *Adv. Mater.* **2022**, *34*, 2204718. [11] Gao, J.; Yu, N.; Chen, Z.; Wei, Y.; Li, C.; Liu, T.; Gu, X.; Zhang, J.; Wei, Z.; Tang, Z.; Hao, X.; Zhang, F.; Zhang, X., Huang, H. Over 19.2% Efficiency of Organic Solar Cells Enabled by Precisely Tuning the Charge Transfer State Via Donor Alloy Strategy. *Adv. Sci.* **2022**, *9*, 2203606. [12] Chen, H.; Zou, Y.; Liang, H.; He, T.; Xu, X.; Zhang, Y.; Ma, Z.; Wang, J.; Zhang, M.; Li, Q.; Li, C.; Long, G.; Wan, X.; Yao, Z., Chen, Y. Lowering the energy loss of organic solar cells by molecular packing engineering via multiple molecular conjugation extension. *Sci. China Chem.* **2022**, *65*, 1362-1373. [13] Zhang, Z.; Li, Y.; Cai, G.; Zhang, Y.; Lu, X., Lin, Y. Selenium Heterocyclic Electron Acceptor with Small Urbach Energy for As-Cast High-Performance Organic Solar Cells. *J. Am. Chem. Soc.* **2020**, *142*, 18741-18745. [14] Zhang, X.; Qin, L.; Liu, X.; Zhang, C.; Yu, J.; Xiao, Z.; Zheng, N.; Wang, B.; Wei, Y.; Xie, Z.; Wu, Y.; Wei, Z.; Wang, K.; Gao, F.; Ding, L., Huang, H. Enhancing the Photovoltaic Performance of Triplet Acceptors Enabled by Side-Chain Engineering. *Sol. RRL* **2021**, *5*, 2100522. [15] Li, S.; Zhan, L.; Liu, F.; Ren, J.; Shi, M.; Li, C.-Z.; Russell, T. P., Chen, H. An Unfused-Core-Based Nonfullerene Acceptor Enables High-Efficiency Organic Solar Cells with Excellent Morphological Stability at High Temperatures. *Adv. Mater.* **2018**, *30*, 1705208. [16] Huang, H.; Guo, Q.; Feng, S.; Zhang, C.; Bi, Z.; Xue, W.; Yang, J.; Song, J.; Li, C.; Xu, X.; Tang, Z.; Ma, W., Bo, Z. Noncovalently fused-ring electron acceptors with near-infrared absorption for high-performance organic solar cells. *Nat. Commun.* **2019**, *10*, 3038. [17] Yu, Z.-P.; Liu, Z.-X.; Chen, F.-X.; Qin, R.; Lau, T.-K.; Yin, J.-L.; Kong, X.; Lu, X.; Shi, M.; Li, C.-Z., Chen, H. Simple non-fused electron acceptors for efficient and stable organic solar cells. *Nat. Commun.* **2019**, *10*, 2152. [18] Gu, X.-B.; Gao, J.-H.; Han, Z.-Y.; Shi, Y.-H.; Wei, Y.-N.; Zhang, Y.-C.; Peng, Q.; Wei, Z.-X.; Zhang, X., Huang, H. A Simple Building

Block with Noncovalently Conformational Locks towards Constructing Low-Cost and High-Performance Nonfused Ring Electron Acceptors. *Chin. J. Polym. Sci.*, DOI: 10.1007/s10118-10022-12888-10119. [19] Li, C.; Zhang, X.; Yu, N.; Gu, X.; Qin, L.; Wei, Y.; Liu, X.; Zhang, J.; Wei, Z.; Tang, Z.; Shi, Q., Huang, H. Simple Nonfused-Ring Electron Acceptors with Noncovalently Conformational Locks for Low-Cost and High-Performance Organic Solar Cells Enabled by End-Group Engineering. *Adv. Funct. Mater.* **2022**, *32*, 2108861. [20] Zhang, X.; Qin, L.; Yu, J.; Li, Y.; Wei, Y.; Liu, X.; Lu, X.; Gao, F., Huang, H. High-Performance Noncovalently Fused-Ring Electron Acceptors for Organic Solar Cells Enabled by Noncovalent Intramolecular Interactions and End-Group Engineering. *Angew. Chem. Int. Ed.* **2021**, *60*, 12475-12481. [21] Zhang, X.; Li, C.; Qin, L.; Chen, H.; Yu, J.; Wei, Y.; Liu, X.; Zhang, J.; Wei, Z.; Gao, F.; Peng, Q., Huang, H. Side-Chain Engineering for Enhancing the Molecular Rigidity and Photovoltaic Performance of Noncovalently Fused-Ring Electron Acceptors. *Angew. Chem. Int. Ed.* **2021**, *60*, 17720-17725. [22] Huang, H.; Chen, Z.; Ortiz, R. P.; Newman, C.; Usta, H.; Lou, S.; Youn, J.; Noh, Y.-Y.; Baeg, K.-J.; Chen, L. X.; Facchetti, A., Marks, T. Combining Electron-Neutral Building Blocks with Intramolecular “Conformational Locks” Affords Stable, High-Mobility P- and N-Channel Polymer Semiconductors. *J. Am. Chem. Soc.* **2012**, *134*, 10966-10973. [23] Huang, H.; Yang, L.; Facchetti, A., Marks, T. J. Organic and Polymeric Semiconductors Enhanced by Noncovalent Conformational Locks. *Chem. Rev.* **2017**, *117*, 10291-10318. [24] Yu, S.; Peng, A.; Zhang, S., Huang, H. Noncovalent conformational locks in organic semiconductors. *Sci. China Chem.* **2018**, *61*, 1359-1367. [25] Zhang, X.; Wei, Y.; Liu, X.; Qin, L.; Yu, N.; Tang, Z.; Wei, Z.; Shi, Q.; Peng, A., Huang, H. Enhancing Photovoltaic Performances of Naphthalene-Based Unfused-Ring Electron Acceptors upon Regioisomerization. *Sol. RRL* **2021**, *5*, 2100094. [26] Zhang, X.; Qin, L.; Li, L.; Liu, X.; Wei, Y., Huang, H. A New Noncovalently Fused-Ring Electron Acceptor Based on 3,7-Dialkyloxybenzo[1,2-b:4,5-b']dithiophene for Low-Cost and High-Performance Organic Solar Cells. *Macromol. Rapid Commun.* **2022**, *43*, 2200085. [27] Liu, Y.; Song, J., Bo, Z. Designing high performance conjugated materials for photovoltaic cells with the aid of intramolecular noncovalent interactions. *Chem. Commun.* **2021**, *57*, 302-314. [28] Yang, M.; Wei, W.; Zhou, X.; Wang, Z., Duan, C. Non-fused ring acceptors for organic solar cells. *Energy Mater.* **2021**, *1*, 100008. [29] Li, Y.; Yu, J.; Zhou, Y., Li, Z. a. Molecular Insights of Non-fused Ring Acceptors for High-Performance Non-fullerene Organic Solar Cells. *Chem. - Eur. J.* **2022**, *28*, e202201675. [30] Wang, Y.; Liu, Z.; Cui, X.; Wang, C.; Lu, H.; Liu, Y.; Fei, Z.; Ma, Z., Bo, Z. Small molecule acceptors with a ladder-like core for high-performance organic solar cells with low non-radiative energy losses. *J. Mater. Chem. A* **2020**, *8*, 12495-12501. [31] Yoon, N.; Jeong, J.-Y.; Oh, S.; Song, C. E.; Lee, H. K.; Shin, W. S.; Lee, J.-C.; Moon, S.-J., Lee, S. K. Effects of Electron-Donating and Electron-Accepting Substitution on Photovoltaic Performance in Benzothiadiazole-Based A-D-A'-D-A-Type Small-Molecule Acceptor Solar Cells. *ACS Appl. Energy Mater.* **2020**, *3*, 12327-12337. [32] Liu, X.; Wei, Y.; Zhang, X.; Qin, L.; Wei, Z., Huang, H. An A-D-A'-D-A type unfused nonfullerene acceptor for organic solar cells with approaching 14% efficiency. *Sci. China Chem.* **2021**, *64*, 228-231. [33] Zhou, X.; Pang, S.; Wu, B.; Zhou, J.; Tang, H.; Lin, K.; Xie, Z.; Duan, C.; Huang, F., Cao, Y. Noncovalent Interactions Induced by Fluorination of the Central Core Improve the Photovoltaic Performance of A-D-A'-D-A-Type Nonfused Ring Acceptors. *ACS Appl. Energy Mater.* **2022**, *5*, 7710-7718. [34] Luo, D.; Jiang, Z.; Yang, W.; Guo, X.; Li, X.; Zhou, E.; Li, G.; Li, L.; Duan, C.; Shan, C.; Wang, Z.; Li, Y.; Xu, B., Kyaw, A. K. K. Dual-functional ambipolar non-fused ring electron acceptor as third component and designing similar molecular structure between two acceptors for high-performance ternary organic solar cells. *Nano Energy* **2022**, *98*, 107186. [35] Geng, S.-Z.; Yang, W.-T.; Gao, J.; Li, S.-X.; Shi, M.-M.; Lau, T.-K.; Lu, X.-H.; Li, C.-Z., Chen, H.-Z. Non-fullerene Acceptors with a Thieno[3,4-c]pyrrole-4,6-dione (TPD) Core for Efficient Organic Solar Cells. *Chin. J. Polym. Sci.* **2019**, *37*, 1005-1014. [36] Li, Y.; Fu, H.; Wu, Z.; Wu, X.; Wang, M.; Qin, H.; Lin, F.; Woo, H. Y., Jen, A. K. Y. Regulating the Aggregation of Unfused Non-Fullerene Acceptors via Molecular Engineering towards Efficient Polymer Solar Cells. *ChemSusChem* **2021**, *14*, 3579-3589. [37] Hu, T.-Y.; Zhang, Y.; Lu, B.-S.; Ma, Y.-F.; Zhu, Y.-N.; Wang, Y.-T.; Zhang, B.-Y.; Zhang, Z.-Q.; Wang, J.; Yang, Y., Zhang, H.-L. Unfused-ring small molecule acceptors based on A1-D-A2-D-A1 architecture with low non-radiative energy loss and excellent air stability. *Mater. Today Energy* **2021**, *21*, 100802. [38] Lin, Y.; Fan, H.; Li, Y., Zhan, X. Thiazole-Based Organic Semiconductors for Organic Electronics. *Adv. Mater.* **2012**, *24*, 3087-3106. [39] Zhang, L.; Deng, W.; Wu, B.; Ye, L.; Sun, X.; Wang, Z.; Gao, K.; Wu, H.; Duan, C.; Huang, F., Cao, Y. Reduced Energy Loss

in Non-Fullerene Organic Solar Cells with Isomeric Donor Polymers Containing Thiazole  $\pi$ -Spacers. *ACS Appl. Mater. Interfaces* **2020**, *12*, 753-762. [40] Ando, S.; Murakami, R.; Nishida, J.-i.; Tada, H.; Inoue, Y.; Tokito, S., Yamashita, Y. n-Type Organic Field-Effect Transistors with Very High Electron Mobility Based on Thiazole Oligomers with Trifluoromethylphenyl Groups. *J. Am. Chem. Soc.* **2005**, *127*, 14996-14997. [41] Jung, I. H.; Jung, Y. K.; Lee, J.; Park, J.-H.; Woo, H. Y.; Lee, J.-I.; Chu, H. Y., Shim, H.-K. Synthesis and electroluminescent properties of fluorene-based copolymers containing electron-withdrawing thiazole derivatives. *J. Polym. Sci. A Polym. Chem.* **2008**, *46*, 7148-7161. [42] Spano, F. C. The Spectral Signatures of Frenkel Polarons in H- and J-Aggregates. *Acc. Chem. Res.* **2010**, *43*, 429-439. [43] Kyaw, A. K. K.; Wang, D. H.; Wynands, D.; Zhang, J.; Nguyen, T.-Q.; Bazan, G. C., Heeger, A. J. Improved Light Harvesting and Improved Efficiency by Insertion of an Optical Spacer (ZnO) in Solution-Processed Small-Molecule Solar Cells. *Nano Lett.* **2013**, *13*, 3796-3801.

Manuscript received: XXXX, 2022 Manuscript revised: XXXX, 2022 Manuscript accepted: XXXX, 2022 Accepted manuscript

## Entry for the Table of Contents

The Combination of S[?]N and S[?]Cl Noncovalently Conformational Locks for Constructing High-Planarity Two A-D-A'-D-A type nonfused-ring electron acceptors (NFREAs) **Tz-H** and **Tz-Cl** were designed and synthesized based

